DEUTSCHES ELEKTRONEN – SYNCHROTRON

DESY 93-057
April 1993

Quantum Eigenstates of a Strongly Chaotic System and the Scar Phenomenon

R. Aurich, F. Steiner
II. Institut für Theoretische Physik, Universität Hamburg

ISSN 0418-9833

NOTKESTRASSE 85 · D-2000 HAMBURG 52

To be sure that your preprints are promptly included in the
HIGH ENERGY PHYSICS INDEX,
send them to (if possible by air mail):

DESY
Bibliothek
Notkestraße 85
W-2000 Hamburg 52
Germany

DESY-IfH
Bibliothek
Platanenallee 6
O-1615 Zeuthen
Germany

DESY 93-057
April 1993

ISSN 0418 - 9833

Quantum Eigenstates of a Strongly Chaotic System and the Scar Phenomenon [1]

by

R. Aurich and F. Steiner

II.Institut für Theoretische Physik , Universität Hamburg
Luruper Chaussee 149 , 2000 Hamburg 50
Federal Republic of Germany

Abstract

The quantum eigenstates of a strongly chaotic system (hyperbolic octagon) are studied with special emphasis on the scar phenomenon. The dynamics of a localized wavepacket is discussed which travels along a short periodic orbit yielding a test for the scar model developed by Heller. The autocorrelation function $C(t)$ and the smeared weighted spectral density $S_T(E)$ are in accordance with this model, but the conclusion that this implies the existence of scarred eigenstates is not confirmed. A random wavefunction model generates with the same probability intensity structures being localized near short periodic orbits as the wavefunctions obeying the Schrödinger equation. Although there are some eigenstates which are localized near a periodic orbit, the conclusion that their intensities differ significantly from the statistically expected ones cannot be drawn. Thus the scar phenomenon seems to be absent in the case of hyperbolic octagons.

[1]Supported by Deutsche Forschungsgemeinschaft under Contract No. DFG-Ste 241/4-6

I Introduction

In this paper we study the quantum eigenstates of a conservative Hamiltonian system with two degrees of freedom having a purely discrete spectrum. The classical counterpart of the quantum system is strongly chaotic, i.e. a K-system. The first predictions on characteristic properties of quantum eigenstates of classically strongly chaotic systems were derived from phase space considerations in which the Wigner function $W(\vec{q},\vec{p})$ [1] plays a crucial role. Since the energy is the only constant of motion, the classical dynamics takes place in phase space on a three dimensional energy surface on which the Wigner function should semiclassically concentrate. This behaviour should occur because of $W(\vec{q},\vec{p}) \to h^N W^2(\vec{q},\vec{p})$ for $h \to 0$ and N degrees of freedom [2], i.e. in the semiclassical limit the Wigner function must either diverge or vanish. Furthermore, the so-called "semiclassical eigenfunction hypothesis" states that the Wigner function semiclassically condenses like a δ-function on the energy surface [3, 4, 5]. The properties of the wavefunctions $\Psi(\vec{q})$ can be obtained by projecting the Wigner function from phase space onto the configuration space. In this way it could be shown that the wavefunctions should not possess caustics like the wavefunctions of integrable systems, and that the autocorrelation function of the wavefunctions should reveal a universal behaviour expressible by Bessel functions [5]. In addition, the amplitude distribution $P(\Psi)$ of the wavefunctions Ψ was conjectured to be a Gaussian [5] which was recently confirmed on numerical grounds [6, 7, 8, 9]. Intuitively one expects an irregular intensity structure of the wavefunctions and "chaotic" nodal lines.

In view of the above semiclassical results on chaotic wavefunctions, Heller's discovery of scarred wavefunctions in the stadium billiard [10] came at a surprise since the scars endow wavefunctions with some special structure. Heller has given the following definition of a scar [11]: "A quantum eigenstate of a classically chaotic system has a *scar* of a periodic orbit if its density on the classical invariant manifolds near the periodic orbit differs significantly from the statistically expected density." Thus a wavefunction possesses a scar if its intensity $|\Psi|^2$ along a periodic orbit is either very high or very low. In addition to the stadium billiard there are some further examples like the hydrogen atom in a magnetic field [12] or the two-center shell-model [13] for which the authors [12, 13] claim the existence of scars.

However not all chaotic systems show the scar phenomenon, a fact to which we have drawn attention already in our previous work [7]. Recently, in numerical studies of wavefunctions in Artin's billiard, i.e. the Maass waveforms of PSL(2,**Z**), no scars on closed geodesics have been observed [9]. In [14] the behaviour of the maximal intensities of eigenstates in dependence of their excitation energy is discussed on a rigorous mathematical basis. These maximal intensities seem to increase so slowly with energy that localization seems to be improbable. Thus the question of scars is far from being settled.

In this paper the wavefunctions of *hyperbolic octagons* are studied with special emphasis on the scar phenomenon. As our main result we show that scarring is absent in our system which thus provides an interesting counter example. In section II a short introduction to our system, the free motion on hyperbolic octagons, is given. Section III provides a summary of the arguments put forward by Heller [11] which yield the theoretical framework of the scar analysis. Section IV is devoted to the computation of the time evolution of a given initial state in a hyperbolic octagon which is then used for a computation of the autocorrelation function $C(t)$ defined in eq.(7) and the smeared weighted level density $S_T(E)$ defined in eq.(11). In section V we present for the first time a theory for $C(t)$ based on periodic-orbit theory using an approximation for $S_T(E)$ which shows that the "zero-length" contribution alone accurately

accounts for $C(t)$ for times t of the order of the revolution time along the periodic orbit. In section VI a random wavefunction model is introduced and compared with the "true" wavefunctions. With respect to the scar phenomenon the random wavefunctions reveal the same behaviour as the "true" wavefunctions. This analysis shows that the accumulation of high intensity structures near short periodic orbits in some eigenstates is not statistically significant, and thus we conclude that the scar phenomenon is absent in the case of hyperbolic octagons.

II Hyperbolic Octagons

The chaotic model that is discussed in this paper is a conservative Hamiltonian system with two degrees of freedom which classically consists of a point particle sliding freely on compact hyperbolic surfaces. The surfaces to be considered are compact Riemann surfaces $\mathcal{F}$ of constant negative Gaussian curvature with genus $g = 2$, i. e. they have the topology of a sphere with two handles. Due to the Gauß-Bonnet theorem, $\mathrm{Area}(\mathcal{F}) = 4\pi(g-1)$, the area of such a surface is $\mathrm{Area}(\mathcal{F}) = 4\pi$. The sphere with two handles can be cut so that one obtains an octagon with geodesic edges, where opposite sides must be identified leading to periodic boundary conditions. A given octagon is mapped into the Poincaré disc $\mathcal{D}$, which consists of the interior of the unit circle in the complex z–plane ($z = x_1 + ix_2$) endowed with the hyperbolic metric

$$g_{ij} = \frac{4}{(1-x_1^2-x_2^2)^2}\delta_{ij} \ , \ i,j = 1,2 \tag{1}$$

corresponding to constant negative Gaussian curvature $K = -1$. (This fixes the length scale.) The hyperbolic distance $d(z,z')$ between two points z and z' is given by

$$\cosh d(z,z') \ := \ 1 + \frac{2|z-z'|^2}{(1-|z|^2)(1-|z'|^2)} \quad . \tag{2}$$

The classical motion (geodesic flow) is determined by the Hamiltonian $H = \frac{1}{2m}p_i g^{ij} p_j$, $p_i = m\, g_{ij}\, dx^j/dt$. The geodesics are circles intersecting the boundary of the Poincaré disc $\mathcal{D}$ perpendicularly.

The quantum mechanical system is governed by the Schrödinger equation

$$-\Delta\Psi_n(z) = E_n\Psi_n(z) \quad , \quad \Delta = \frac{1}{4}(1-x_1^2-x_2^2)^2\left(\frac{\partial^2}{\partial x_1^2}+\frac{\partial^2}{\partial x_2^2}\right) \quad , \tag{3}$$

where we used $\hbar = 2m = 1$. The periodic boundary conditions are realized by identifying the points z and $z' \equiv b(z)$,

$$b(z) := \frac{\alpha z + \beta}{\beta^* z + \alpha^*} \ , \ |\alpha|^2 - |\beta|^2 = 1 \ , \tag{4}$$

where the "boosts"

$$b = \begin{pmatrix} \alpha & \beta \\ \beta^* & \alpha^* \end{pmatrix} \in \mathrm{SU(1,1)}/\{\pm 1\}$$

are chosen such that they map a given edge onto the opposite edge. Four boosts are sufficient for the description of a given octagon. These four boosts and their inverses are the generators of the Fuchsian group Γ which tessellates the Poincaré disc $\mathcal{D}$. The solutions of the Schrödinger equation (3) have to obey the periodic boundary conditions

$$\Psi(z) = \Psi(b(z)) \quad \text{for all} \quad b \in \Gamma \ , \tag{5}$$

and are normalized according to

$$\int\!\!\int_{\mathcal{F}} dx_1\, dx_2 \, \frac{4}{(1-x_1^2-x_2^2)^2}\, \Psi_m^*(z)\Psi_n(z) \ = \ \delta_{mn} \quad . \tag{6}$$

For more details of this model, see the well–written introductions in [15, 16] and our earlier papers [17, 18, 7, 8, 22, 23].

The quantum eigenstates of hyperbolic octagons were already investigated in [7, 8]. In [7] an exact orbit theory for the quantum eigenstates was derived and applied. It allows the computation of a few low lying eigenstates in terms of classical orbits. This theory is an exact version of Bogomolny's semiclassical scar theory [19] which yields the semiclassical contributions of classical orbits to quantum wavefunctions. The description of highly excited wavefunctions by this orbit theory is practically not possible since the number of required orbits increases exponentially with the excitation energy of the state. For the computation of the first few excited eigenstates only a limited number of orbits is needed and one observes a scar phenomenon: eigenstates with positive parity develop the strongest intensities in the neighbourhood of the first few periodic orbits, whereas eigenstates with negative parity possess nodal lines there. However, this scar phenomenon is limited to the eigenstates with energy $E < 10$. For higher excited states too many orbits contribute collectively so that no connection to a single orbit survives, and no scars are expected from the orbit theory. In principle one cannot exclude the possibility that an unknown miraculous mechanism exists by which very long orbits enhance the contribution of a special short orbit. This would correspond to the bootstrapping effect in the framework of periodic orbit theory [20]. However, the purpose of this paper is to demonstrate that such a mechanism seems not to exist and no scars occur in highly excited eigenstates. The statistical properties of highly excited eigenstates were already discussed in [8] where it was shown that the amplitude distribution $P(\Psi)$ is a Gaussian and that the circular–wave expansion coefficients of the eigenstates behave like pseudo–random numbers. These properties support the picture of irregular wavefunctions without any order enforced by periodic orbits. The eigenstates discussed in [8] were computed using the boundary–element method. The same method was employed to compute all eigenstates of positive parity with energy between $E = 1500$ and $E = 2140$ for the asymmetric hyperbolic octagon defined by the following corner points $z_k = r_k e^{i\varphi_k}$ in the Poincaré disc: $r_1 = 0.9405185836$, $\varphi_1 = 0$, $r_2 = 0.8701653$, $\varphi_2 = 0.8023654$, $r_3 = 0.7609273$, $\varphi_3 = 2.1175027$, $r_4 = 0.8575482$, $\varphi_4 = 2.5846103$, where the other 4 corner–points are obtained from these by the parity transformation $z \to -z$ (see also figure 4). There are 317 eigenstates with positive parity in this energy interval constituting the basis of our scar analysis.

III The scar model

In this section we would like to briefly review the arguments given by Heller [10, 11] which force some quantum eigenstates to be scarred by short periodic orbits. One considers a Gaussian wavepacket $\Psi_G(z,t)$ which moves along a short periodic orbit of the given chaotic billiard. The expectation values of position and momentum are governed by the Ehrenfest theorem and thus obey the laws of classical dynamics, and the wavepacket $\Psi_G(z,t)$ revolves along the given periodic orbit. Now consider the overlap integral

$$C(t) \ := \ \langle\, \Psi_G(z,0) \,|\, \Psi_G(z,t) \,\rangle \tag{7}$$

which should show as a function of time t peaks with period $T = \frac{l}{2p}$ corresponding to the multiple traversals of the wavepacket, where l is the length of the periodic orbit. Since the wavepacket spreads, the amplitude of the peak declines after each traversal. The decline is determined in the case of chaotic systems by the *time–dependent* Liapunov exponent λ of the classical periodic orbit according to $e^{-\lambda t/2}$ [11]. Expanding the wavepacket at time $t = 0$ with respect to the normalized quantum eigenstates $\Psi_n(z)$

$$\Psi_G(z,0) \;=\; \sum_{n=0}^{\infty} c_n\, \Psi_n(z) \tag{8}$$

yields for (7) the expansion

$$C(t) \;=\; \sum_{n=0}^{\infty} |c_n|^2\, e^{-iE_n t} \quad , \quad C(0) \;=\; \sum_{n=0}^{\infty} |c_n|^2 \;=\; 1 \quad . \tag{9}$$

The Fourier transform of $C(t)$ with respect to energy E yields the spectral density $S(E)$ weighted by the probabilities $|c_n|^2$

$$S(E) \;:=\; \frac{1}{2\pi} \int_{-\infty}^{\infty} dt\; C(t)\, e^{iEt} \;=\; \sum_{n=0}^{\infty} |c_n|^2\, \delta(E - E_n) \quad . \tag{10}$$

If the t–integration in (10) is carried out only over the interval $[-\mathcal{T}, \mathcal{T}]$ one obtains a smeared weighted spectral density

$$S_{\mathcal{T}}(E) \;:=\; \frac{1}{2\pi} \int_{-\mathcal{T}}^{\mathcal{T}} dt\; C(t)\, e^{iEt} \;=\; \sum_{n=0}^{\infty} |c_n|^2\, \frac{\sin(\,(E_n - E)\mathcal{T})}{\pi\,(E_n - E)} \tag{11}$$

where the energy resolution ΔE is roughly given by $\Delta E = \frac{2\pi}{\mathcal{T}}$. The crucial point is that the Fourier transform of a function which shows peaks at a period T with a decline proportional to $e^{-\lambda t/2}$ has peaks of width λ with a spacing $\omega := \frac{2\pi}{T}$. Thus if $C(t)$ is known up to $\mathcal{T}^* \simeq \frac{2\pi}{\lambda}$ the Fourier transform $S_{\mathcal{T}^*}(E)$ should already show this feature. If the width is much smaller than the distance between the peaks, i.e. $\lambda \ll \omega$, only the eigenstates which are lying in these "bands" contribute to the expansion of the wavepacket. Since the wavepacket shows an enhanced intensity only along the periodic orbit this must carry over to the properties of the contributing quantum eigenstates, which are then scarred by the periodic orbit. This argumentation requires that the wavepacket is sufficiently localized after the time $\mathcal{T}^*$ because a wavepacket which is spread after $\mathcal{T}^*$ over the whole periodic orbit interferes with itself and does not produce the required "periodicity" of $C(t)$.

The relative enhancement of the probabilities $|c_n|^2$ within such a band is of the order $\frac{\omega}{\lambda}$. However, there are $N_b = \lambda \overline{d}(E)$ quantum eigenstates within such a band, where $\overline{d}(E)$ is the mean level density. If the number N_b of contributing eigenstates is too large, the above argumentation is flawed, since the localization of the wavepacket is only collectively reproduced by the N_b eigenstates and a one to one correspondence is missing. In other words, since too many eigenstates produce the strong intensity near the periodic orbit, an individual eigenstate does not need to show a significant intensity deviation from the statistically expected one, and scarring is absent. In the following we will see that this happens, indeed, in the case of hyperbolic octagons where no scarred eigenstates occur.

IV Wavepacket dynamics in hyperbolic octagons

To scrutinize Heller's argumentation it is necessary to consider the dynamics of a suitable wavepacket in our model, the hyperbolic octagon. The time evolution of a given initial state is completely determined by the Feynman kernel $K(z, z'; t)$ which can be expanded with respect to the quantum eigenstates of the system

$$K(z, z'; t) \;=\; \sum_{n=0}^{\infty} e^{-iE_n t}\, \Psi_n(z)\, \Psi_n^*(z') \quad . \tag{12}$$

A representation of the Feynman kernel can be obtained from the exact sum rule for wavefunctions derived in our previous paper [7]

$$\sum_{n=0}^{\infty} h(p_n) \Psi_n(z) \Psi_n^*(z') \;=\; \frac{1}{2\pi} \sum_{b \in \Gamma} \int_0^{\infty} dp\; p \tanh(\pi p)\; h(p)\; P_{-\frac{1}{2}+ip}(\cosh d(z, b(z'))) \quad , \tag{13}$$

where $P_{-\frac{1}{2}+ip}(\cosh \tau)$ denotes the Legendre function and $h(p)$ an arbitrary function satisfying the three (sufficient) conditions:

- $h(p) = h(-p)$,
- $h(p)$ is holomorphic in the strip $|\mathrm{Im} p| \leq \frac{1}{2} + \varepsilon, \varepsilon > 0$,
- $h(p) = O(p^{-2-\delta}), \delta > 0$, for $|p| \to \infty$.

With the choice

$$h(p) \;=\; \exp(-i\,E\,t) \quad , \quad E \;=\; p^2 + \frac{1}{4} \quad , \tag{14}$$

eq.(13) yields the following representation of the Feynman kernel

$$K(z, z'; t) \;=\; \frac{1}{2\pi} \sum_{b \in \Gamma} \int_0^{\infty} dp\; p\; \tanh(\pi p)\; e^{-i(p^2 + \frac{1}{4})t}\; P_{-\frac{1}{2}+ip}(\cosh d(z, b(z'))) \quad . \tag{15}$$

Without the summation over the Fuchsian group Γ, the free Feynman kernel of the Poincaré disc ($\tau := d(z, z')$)

$$K_0(\tau; t) \;=\; \frac{1}{2\pi} \int_0^{\infty} dp\; p\; \tanh(\pi p)\; e^{-i(p^2 + \frac{1}{4})t}\; P_{-\frac{1}{2}+ip}(\cosh \tau) \tag{16}$$

is obtained. The Legendre function $P_{-\frac{1}{2}+ip}(\cosh \tau)$ can be computed from the integral representation

$$P_{-\frac{1}{2}+ip}(\cosh \tau) \;=\; \frac{\sqrt{2}}{\pi} \int_0^{\tau} \frac{\cos(pt)\; dt}{\sqrt{\cosh \tau - \cosh t}} \quad . \tag{17}$$

However, for a numerical evaluation of the Feynman kernel eq.(15) is hardly adapted since the amplitude of oscillations of the integrand in (15) grows like $\sqrt{p}$ as can be inferred from the asymptotic behaviour of $P_{-\frac{1}{2}+ip}(\cosh \tau)$

$$P_{-\frac{1}{2}+ip}(\cosh \tau) \;\sim\; \sqrt{\frac{2}{\pi p \sinh \tau}}\; \sin(p\tau + \frac{\pi}{4}) \;:=\; f(p) \quad , \quad p \to \infty \quad . \tag{18}$$

This drawback is reflected by the fact that the chosen $h(p)$, eq.(14), does not satisfy the third sufficient condition stated after (13). A numerically suitable expression can be derived by exploiting the asymptotic behaviour (18)

$$K_0(\tau;t) \;=\; \frac{1}{2\pi}\int_0^\infty dp\; p\; e^{-i(p^2+\frac{1}{4})t}\;\Big(\;\tanh(\pi p)\,P_{-\frac{1}{2}+ip}(\cosh\tau) - f(p)\;\Big) \;+\; I(\tau;t) \quad , \qquad (19)$$

where

$$I(\tau;t) \;:=\; \frac{1}{2\pi}\int_0^\infty dp\; p\; f(p)\; e^{-iEt} \;=\; \frac{e^{i(\tau^2/(4t)-t/4)}}{2\pi\sqrt{2\sinh\tau}(it)^{3/4}}\,U\left(-\frac{1}{4};\frac{1}{2};\frac{\tau^2}{4it}\right) \quad . \qquad (20)$$

Here $U(-1/4;1/2;z)$ is a Kummer function which can be expressed by the confluent hypergeometric function ${}_1F_1(a;b;z)$ [21]

$$U\left(-\frac{1}{4};\frac{1}{2};z\right) \;=\; \frac{1}{\sqrt{2\pi}}\left\{\frac{1}{2}\sqrt{z}\Gamma(1/4)\,{}_1F_1\left(\frac{1}{4};\frac{3}{2};z\right) \;+\; \Gamma(3/4)\,{}_1F_1\left(-\frac{1}{4};\frac{1}{2};z\right)\right\} \quad . \qquad (21)$$

The asymptotic behaviour of (19) is determined by the asymptotic behaviour of $U(-1/4;1/2;z)$ [21] ($|z|\to\infty$)

$$U\left(-\frac{1}{4};\frac{1}{2};z\right) \;\sim\; z^{1/4} + O\left(\frac{1}{|z|^{3/4}}\right) \qquad (22)$$

which leads to the semiclassical approximation ($t \ll \tau^2/4$)

$$K_0(\tau;t) \;\simeq\; \frac{1}{4\pi it}\sqrt{\frac{\tau}{\sinh\tau}}\;e^{i\left(\frac{\tau^2}{4t}-\frac{t}{4}\right)} \quad . \qquad (23)$$

In figure 1 a comparison is shown between the Feynman kernel computed from (19) and the semiclassical approximation (23). The agreement is nearly perfect, and in our time–evolution computations the semiclassical approximation (23) is used. A generalization to arbitrary dimensions has been derived in [22].

It is interesting to compare this semiclassical approximation with the exact Feynman kernel of the free particle in the Euclidean plane which is

$$K_0^E(\tau;t) \;=\; \frac{1}{4\pi it}\;e^{i\frac{\tau^2}{4t}} \quad , \qquad (24)$$

again for $\hbar = 1$ and $2m = 1$. One observes that the hyperbolic kernel (23) has (besides the phase factor $e^{-it/4}$) an additional factor $\sqrt{\frac{\tau}{\sinh\tau}}$ which can be interpreted as a factor compensating the hyperbolic metric. Considering polar coordinates (τ,ϕ), the invariant volume element of the hyperbolic plane is $d\mu = \sinh\tau d\tau d\phi$, whereas the one of the Euclidean plane is $d\mu' = \tau d\tau d\phi$, of course. Thus the ratio with which a source at a distance τ acts in the Euclidean case compared to the same situation in the hyperbolic case is given by $\frac{d\mu'}{d\mu} = \frac{\tau}{\sinh\tau}$. Since the prefactor in the Feynman kernel can be interpreted as the square root of the classical probability, the full factor is understood.

According to Heller's argumentation one should consider a localized wavepacket which moves along a short periodic orbit. We choose the second shortest periodic orbit in our hyperbolic octagon, a periodic orbit with length $l_2 = 2.20527\ldots$ which obeys the scarring condition $l < 2\pi$. In the Poincaré disc this periodic orbit intersects the origin $z = 0$ at an angle $\vartheta = 1.210798541\ldots$, see the full line in figure 4. The wavepacket is constructed by multiplying the

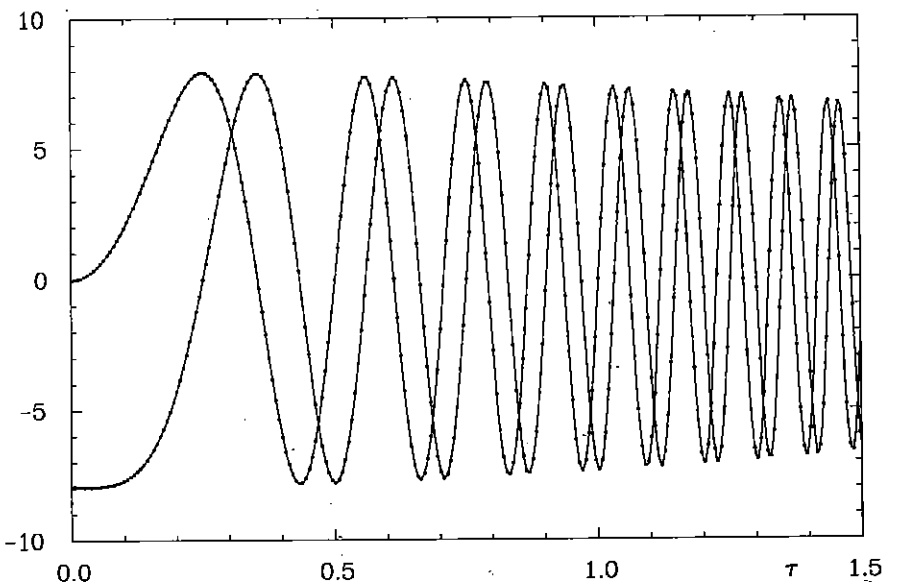

Figure 1: Real and imaginary part of the semiclassical approximation (23) for the Feynman kernel $K_0(\tau;t)$ are shown as full curves as a function of τ for $t = 0.01$. The small dots denote the results obtained from the exact regularized formula (19). Excellent agreement is observed.

Gaussian distribution $\exp\left(-\frac{\tau^2}{4a^2}\right)$ with a plane wave according to the hyperbolic metric. For a sufficiently small parameter a a localized wavepacket is obtained moving in the direction of the plane wave. A plane wave moving with momentum p through the origin $z = 0$ in the Poincaré disc has the representation [16]

$$E_p(\rho,z) \;=\; \left[\frac{1-|z|^2}{|z-\rho|^2}\right]^{\frac{1}{2}+ip} \;=\; \left[\frac{1}{\cosh\tau - \sinh\tau\cos(\phi-\vartheta)}\right]^{\frac{1}{2}+ip} \quad , \qquad (25)$$

where $z = \tanh\frac{\tau}{2}\,e^{i\phi}$, and $\rho = e^{i\vartheta}$ is the point at infinity ($|z| = 1$) at which the plane wave arises at the boundary of the Poincaré disc. Thus the wavepacket with the initial form

$$\Psi_G(z,t=0) \;=\; c\;\exp\left\{-\frac{\tau^2}{4a^2} - \left(\frac{1}{2}+ip\right)\ln\left[\cosh\tau - \sinh\tau\cos(\phi-\vartheta)\right]\right\} \quad , \quad z\in\mathcal{F} \quad , \qquad (26)$$

moves in the direction defined by the angle ϑ. The wavepacket must be sufficiently strongly localized within the considered octagon $\mathcal{F}$ so that $\Psi_G(z,t=0)$ is negligible near the boundary of the octagon, since the initial state must obey the periodic boundary conditions determined by the Fuchsian group Γ. The periodic–boundary condition is then enforced by considering the initial state (26) only within the octagon $\mathcal{F}$, and by transforming every point outside $\mathcal{F}$ according to Γ into the octagon. For such a localized state the normalization constant c is given by

$$c \;=\; \frac{1}{\sqrt{a\pi\sqrt{2\pi}\;e^{a^2/2}\,\mathrm{erf}(a/\sqrt{2})}} \quad . \qquad (27)$$

The quantum eigenstates of hyperbolic octagons can always be classified by parity symmetry, i.e. $\Psi_n^{\pm}(-z) = \pm\Psi_n^{\pm}(z)$. It is thus convenient to consider initial states with a fixed parity. The restriction to a desymmetrized spectrum also enhances the probability to detect a scarred quantum eigenstate, since, as already emphasized, the number N_b of contributing states within a band is $N_b = \lambda\overline{d}(E)$. Thus the level density $\overline{d}(E)$ is reduced by a factor of two by restricting to a single parity class, and the "burden" to generate a high intensity near the periodic orbit is shared by only half of the number of states. The Liapunov exponent λ is, as a classical quantity, not affected by the desymmetrization process. The following wavefunction

$$\Psi_G^{\pm}(z, t=0) \;=\; \frac{1}{\sqrt{2}}\;\{\;\Psi_G(z, t=0) \;\pm\; \Psi_G(-z, t=0)\;\} \qquad (28)$$

defines an initial state with definite parity.

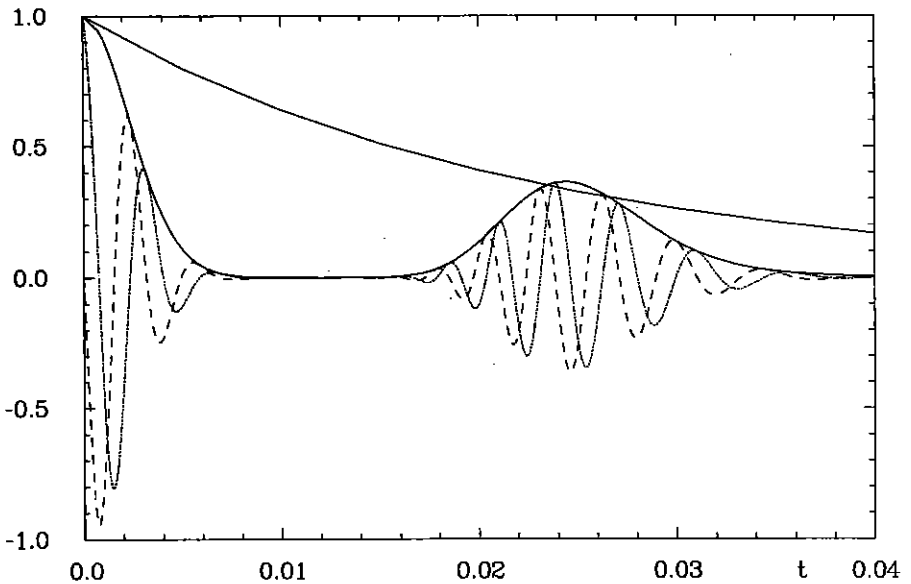

Figure 2: The autocorrelation function $C(t)$ is shown for the wavepacket travelling along the second shortest periodic orbit as discussed in the text. The real part of $C(t)$ is displayed as a dotted curve and the imaginary part as a dashed curve. The lower full curve shows $|C(t)|$, whereas the upper full curve represents $e^{-\lambda t/2}$.

For our numerical evaluation we have chosen the case with positive parity. The wavepacket has a width of $a = 0.1$ and an energy of $E = 2000$. The evolution of the wavepacket has been computed by using the time–evolution equation

$$\Psi_G(z,t) \;=\; \int_{\mathcal{F}} d\mu(z')\;\Psi_G(z',0)\;K(z,z';t) \qquad (29)$$

up to $t = 0.04$ corresponding to roughly 1.5 revolutions around the periodic orbit. The resulting autocorrelation function $C(t)$ defined in eq.(7) is shown in figure 2. After the first decline of

$C(t)$ the wavepacket shows practically no overlap with its initial state. Then the wavepacket returns to its starting point at $t \simeq 0.025$ leading to an increased overlap followed by a further decline. The smooth declining curve in figure 2 corresponds to the expected decline $e^{-\lambda t/2}$, which is thus roughly confirmed by our numerical computation.

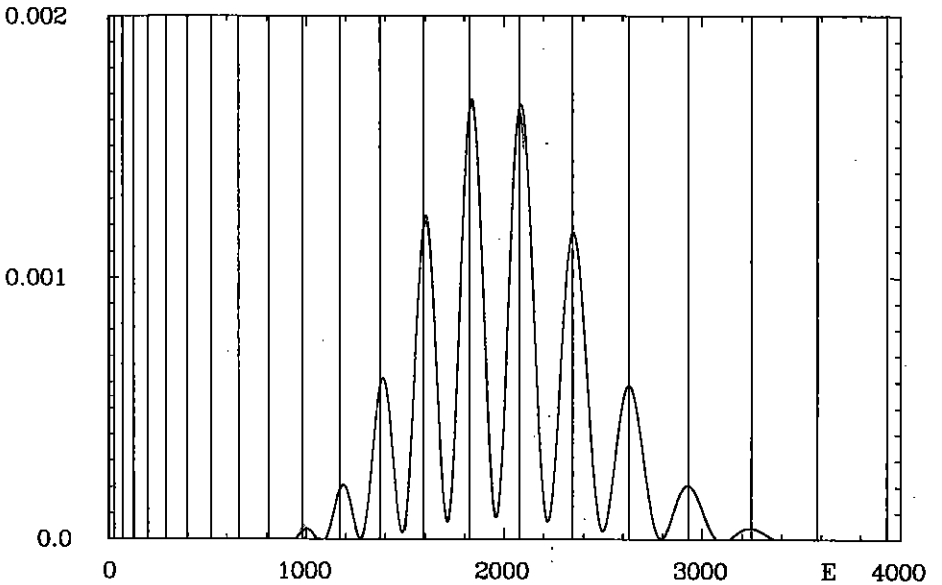

Figure 3: The Fourier transform $S_{\mathcal{T}}(E)$ of $C(t)$ is shown as a full curve. In the interval between $E = 1500$ and $E = 2140$ the smoothed spectral density computed from the quantum eigenstates via the second relation in (11) is shown as a dotted curve.

Knowing $C(t)$ up to $\mathcal{T} = 0.04$, the smeared weighted spectral density $S_{\mathcal{T}}(E)$ can be computed using (11). The result is shown in figure 3, where one observes the expected band structure which is centered around the energy $E = 2000$, i.e. the energy of the wavepacket. In addition, the expansion coefficients c_n have been computed from the eigenstates in the energy interval $E \in [1500, 2140]$ which also yield $S_{\mathcal{T}}(E)$ by (11). This evaluation is also presented in figure 3 as a dotted curve. The agreement is excellent and no deviation is visible except near $E = 1500$ and $E = 2140$ where the contributions of the eigenstates lying outside the considered interval are not negligible due to the finite value of $\mathcal{T}$. Most interesting are the locations of the bands whose positions are in agreement with a kind of modified Bohr–Sommerfeld quantization rule for the *bands* instead for *single* quantal levels. The simple requirement that a band occurs when the length l_n of the periodic orbit is a multiple of the de Broglie wavelength $\lambda_B = \frac{2\pi}{p}$, leads to the "band–quantization" condition

$$p_N \;=\; \frac{2\pi N}{l_n} \quad , \qquad (30)$$

where $N = 1, 2, 3, \ldots$ is the "band–quantum number". The perpendicular lines in figure 3 show the energies of the bands associated with the length l_2, and striking agreement is observed.

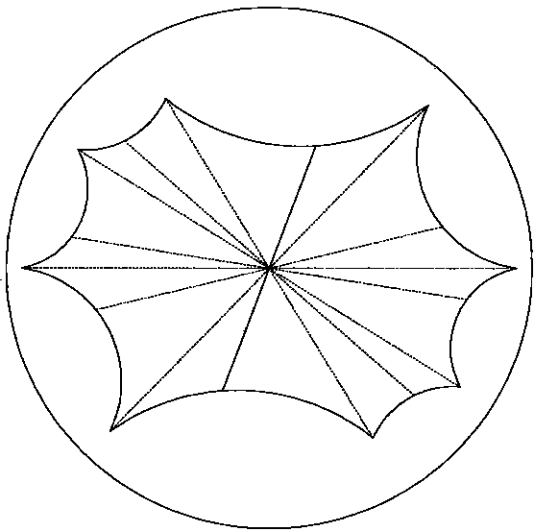

Figure 4: The eight simplest geodesics are shown in the Poincaré disc. They intersect each other at the origin $z = 0$. The shortest one, which plays the crucial role in this paper, is shown as a full line. See also table 1.

It is interesting to consider localized wavepackets which start again at the origin $z = 0$ in the Poincaré disc but in different directions defined by the angle ϑ in eq.(26). Then one expects for $S_T(E)$ a band structure if the angle ϑ lies near an angle belonging to a short periodic orbit and no structure if it is far away from these angles. There are eight simple periodic orbits which cross the origin $z = 0$, see figure 4. Four of these are the straight lines connecting opposite corner points of the octagon. The other four are the connection lines of the midpoints of opposite edges of the octagon. The angles at which these periodic orbits intersect the origin $z = 0$ are listed together with the lengths of the periodic orbits in table 1. In figure 5 the smeared weighted spectral density $S_T(E)$ is shown in dependence of the angle ϑ at which the wavepacket starts. $S_T(E)$ is obtained from eq.(11) for $T = 0.04$ by computing the overlap c_n of the wavepacket with the eigenstates in the energy interval $E = 1500$ to $E = 2140$. The most pronounced band structure occurs at $\vartheta \simeq 1.21$, and a view at table 1 reveals that this angle corresponds indeed to the shortest periodic orbit crossing the origin $z = 0$. It is exactly the periodic orbit which has been discussed above. The second shortest periodic orbit with length $l = 3.303\ldots$ and angle $\vartheta = 0.23\ldots$ shows already a much less pronounced band structure although it safely obeys the scarring condition $l < 2\pi$. The longer the periodic orbit the more diminishes the band structure and thus the probability of scarring of the eigenstates. This result justifies our choice to use the periodic orbit at $\vartheta \simeq 1.21$ for our scar analysis since it shows all the properties predicted by the scar model.

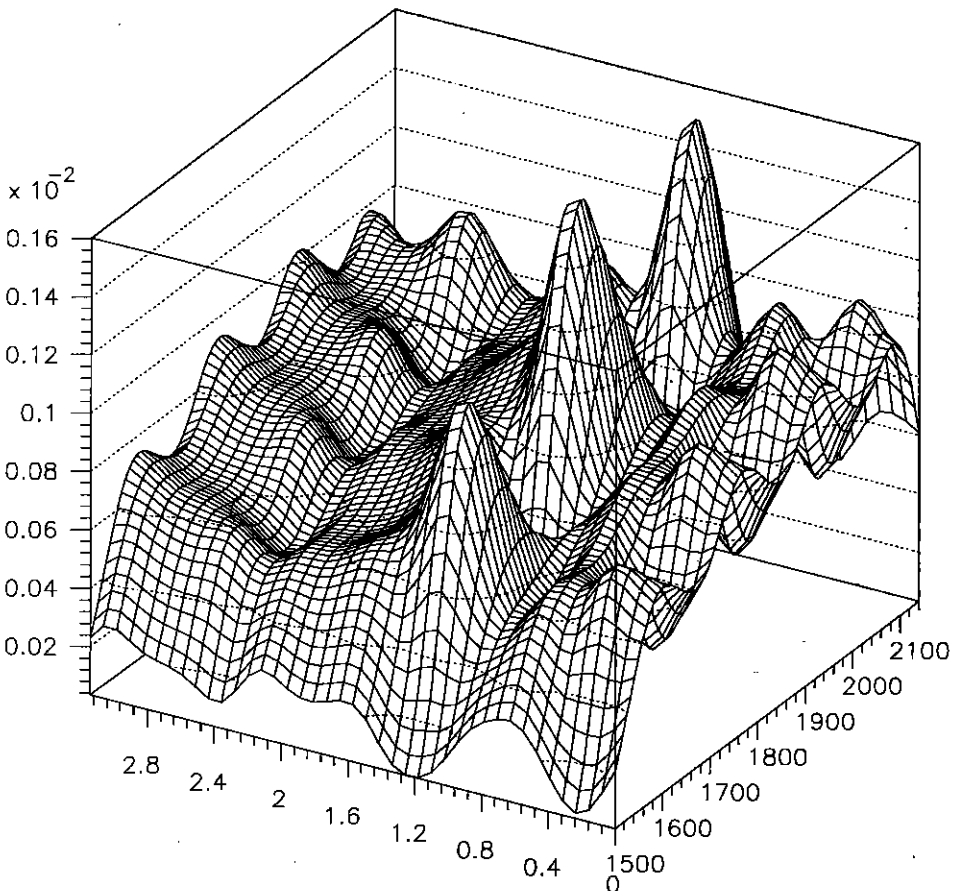

Figure 5: The smeared weighted spectral density $S_T(E)$ is shown in the energy range E=1500 to E=2140 in dependence of the angle $\vartheta \in [0, \pi]$ at which the Gaussian wavepacket starts at the origin in the Poincaré disc.

V Periodic–orbit theory for $C(t)$

In this section a periodic–orbit expression for $C(t)$ is derived from $|c_n|^2 = F(p_n)$, where $F(p)$ approximates the band structure of $S_T(E)$ found in the last section. This expression shows that from the point of view of periodic–orbit theory the main contribution of the recurrence behaviour of $C(t)$ arises from the Thomas–Fermi term, i. e. the so–called "zero–length" term, and not from the periodic–orbit contribution of the second shortest periodic orbit with length l_2. We express an approximation to $S_T(E)$, which itself is expressed in terms of the quantal energies, by the periodic–orbit formula which then allows to find the dominant contribution.

The coarsest structures of $S_T(E)$ are determined by the short time behaviour of $C(t)$. The maxima of the bands of $S_T(E)$ are superimposed on a Gaussian whose width is completely determined by the width a of the initial Gaussian wavepacket and its momentum p. Since only the behaviour at shortest times is required, it suffices to consider the wavepacket in the Euclidean

ϑ	l
0.00000000	6.97009319
0.23761642	3.30340299
0.80236540	5.33504000
1.21079854	2.20527103
2.11750270	3.99365627
2.41849784	3.77084538
2.58461030	5.13601806
2.98568650	4.00481241

Table 1: The angles ϑ and the lengths l of the eight simplest periodic orbits crossing the origin $z = 0$ in the Poincaré disc are given. See also figure 4.

metric, which then allows analytical computations. Starting with a Gaussian wavepacket of width a and momentum p in the Euclidean plane, one obtains $S(E) \sim E^{-1/4}\, e^{-2\,a^2\,(\sqrt{E}-p)^2}$. This determines also the envelope of the bands in the hyperbolic case. With the band–quantization condition $p_N = \frac{2\pi N}{l_2}$ we thus obtain as an approximation to $S_T(E')$ the function

$$F(p') \;=\; \widehat{N}\, e^{-2\,a^2(p-p')^2} \sum_{N=1}^{\infty} e^{-\alpha(p_N-p')^2} \;+\; \widehat{N}\, e^{-2\,a^2(p+p')^2} \sum_{N=1}^{\infty} e^{-\alpha(p_N+p')^2} \qquad (31)$$

where p is again the momentum of the wavepacket. The second term in eq.(31) has been added in order to obtain an even function as it is required by the Selberg trace formula. The width of the bands is denoted by α, which is the only free parameter, and $\widehat{N}$ is a normalization constant which is determined by the constraint

$$\int_0^{\infty} dE\; S_T(E) \;= 1 \quad . \qquad (32)$$

In figure 6 a comparison is shown between the function S_T obtained from the time–evolution of the Gaussian wavepacket and our ansatz $F(p)$. We conclude that the coarse structure is well approximated apart from the fact that the bands at higher energies are somewhat overestimated which is caused by neglecting the factor $E^{-1/4}$ in the ansatz (31), which is, however, convenient in order to obtain manageable expressions. With the approximation $F(p)$ it is now possible to write down the periodic–orbit expression for $C(t)$ by using the Selberg trace formula which is identical to Gutzwiller's periodic–orbit theory in the case of hyperbolic octagons.

The Selberg trace formula for distinct parity classes reads [23]

$$\sum_{n=0}^{\infty} h(p_n^{\pm}) \;=\; \frac{1}{2}\int_{-\infty}^{\infty} dp\; p\, \tanh(\pi p)\, h(p) \;\pm\; \frac{3}{4}\int_{-\infty}^{\infty} dp\, \frac{h(p)}{\cosh \pi p}$$

$$+ \sum_{\{l_n\}} \sum_{k=1}^{\infty} \frac{\chi^{\pm}(l_n)^k\, l_n}{2 \sinh \frac{k\, l_n}{2}}\, g(k\, l_n) \quad . \qquad (33)$$

Here the function $h(p)$ has to obey the same conditions as in the sum–rule (13) for the wavefunctions. The characters $\chi^{\pm}(l_n)$ of the periodic orbits with lengths l_n obey $\chi^{+}(l_n) = +1$ in the case of positive parity. The Fourier transform of $h(p)$ is denoted by $g(x)$. With the choice

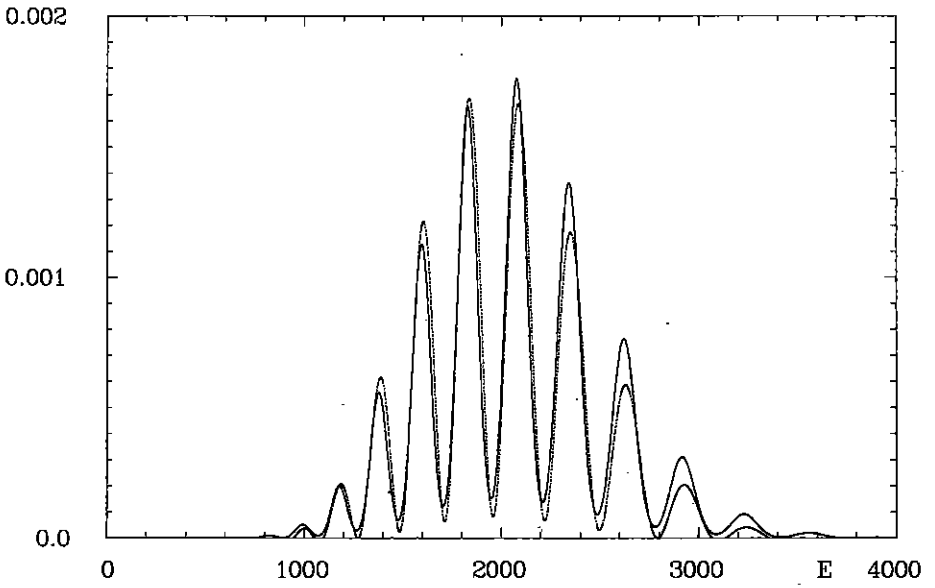

Figure 6: The ansatz $F(p)$, eq.(31), is shown for $\alpha = 1.55$ (full curve) in comparison with $S_T(E)$ obtained from the time–evolution of the Gaussian wavepacket (dotted curve).

$h(p') = F(p')\exp\{-i(p'^2 + \frac{1}{4})t\}$ one obtains an exact periodic–orbit formula for $C(t)$,

$$C(t) \;=\; \sum_{n=0}^{\infty} |c_n|^2\, e^{-E_n^+ t} \;=\; \sum_{n=0}^{\infty} F(p_n^+)\, e^{-ip_n^{+2}t - it/4} \;=\; \sum_{n=0}^{\infty} h(p_n^+) \quad , \qquad (34)$$

which belongs to a wavepacket with probabilities $|c_n|^2 = F(p_n^+)$. The resulting periodic–orbit formula reads in the semiclassical limit $p \to \infty$

$$C(t) \;=\; \frac{2\,\widehat{c}}{\alpha+\beta+it} \sum_{N=1}^{\infty} e^{-\alpha p_N^2} \left\{1 - \sqrt{\pi}\rho e^{\rho^2}\mathrm{erfc}(\rho)\right\}$$

$$+ \frac{3\widehat{c}\sqrt{\pi}}{\sqrt{\alpha+\beta+it}} \sum_{N=1}^{\infty} e^{-\alpha p_N^2} \left\{ e^{\gamma_+^2}\mathrm{erfc}(\gamma_+) \;+\; e^{\gamma_-^2}\mathrm{erfc}(\gamma_-) \right\}$$

$$+ \frac{\widehat{c}}{\sqrt{\pi(\alpha+\beta+it)}} \sum_{N=1}^{\infty} e^{-\alpha p_N^2}$$

$$\times \sum_{\{l_n\}} \sum_{k=1}^{\infty} \frac{l_n}{2\sinh\frac{kl_n}{2}} \left[\exp\left(\frac{(\alpha p_N + \beta p + i\frac{kl_n}{2})^2}{\alpha+\beta+it}\right) \;+\; \exp\left(\frac{(\alpha p_N + \beta p - i\frac{kl_n}{2})^2}{\alpha+\beta+it}\right) \right] \qquad (35)$$

with $\widehat{c} = \frac{1}{2}\widehat{N}e^{-it/4}e^{-\beta p^2}$, $\rho = -\frac{\alpha p_N + \beta p}{\sqrt{\alpha+\beta+it}}$ and $\gamma_{\pm} = \frac{\pi/2 \pm \alpha p_N \pm \beta p}{\sqrt{\alpha+\beta+it}}$, $\beta = 2\,a^2$. A close inspection of eq.(35) reveals that for times t of the order of the revolution time the dominant contribution

comes from the first term on the right hand side of (35) corresponding to the zero–length term. Only for times t much larger than the revolution time the contribution of the periodic orbits becomes important. Thus the short time behaviour is completely determined by the zero–length term and by the band–quantization condition which turns out to be the crucial ingredient. Using the asymptotics of the error–function erfc(z) the following approximation, valid for short times, is obtained

$$C(t) \simeq \frac{4\widehat{c}\sqrt{\pi}}{(\alpha+\beta+it)^{3/2}} \sum_{N=1}^{\infty} (\alpha p_N + \beta p) \exp\left(-\frac{\alpha\beta(p_N-p)^2 + it(\alpha p_N^2 + \beta p^2)}{\alpha+\beta+it}\right) . \quad (36)$$

The real and imaginary part of eq.(36) are shown in figure 7 as full curves in comparison with $C(t)$ (dotted curves) obtained from the time–evolution of the wavepacket. (The formulae in this section are valid for eigenstates normalized with respect to half an octagon being the fundamental domain for a fixed parity class. The eigenstates in the remaining parts of the paper are normalized according to eq.(6). In figure 7 the resulting factor of 2 has been corrected.) The agreement is striking, and we would like to note that the zero–length term knows nothing about the given octagon apart of the length of a single periodic orbit, because the zero–length term is the same for all octagons. The given octagon is encoded in the length spectrum of the periodic orbits entering the periodic–orbit sum, but not in the zero–length term.

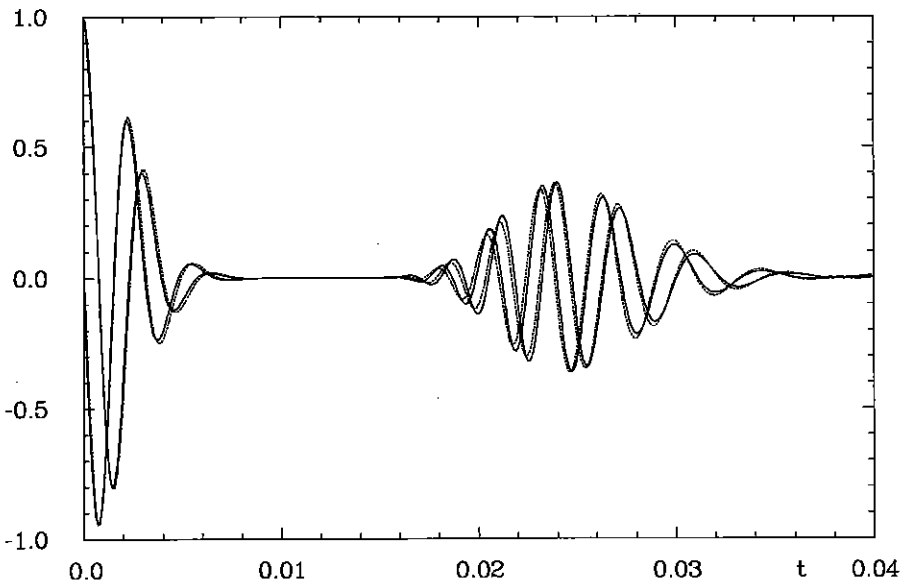

Figure 7: Real and imaginary part of the zero–length contribution (36) (full curves) of the periodic–orbit theory are shown together with the "true" $C(t)$ (dotted curves).

VI A random wavefunction model

In the preceding sections we have shown that the probabilities $|c_n|^2$ are indeed distributed according to the model based on wavepacket dynamics. The best scar candidates among the quantum eigenstates should therefore lie under those bands which have the largest probabilities. In figure 8 the probabilities $|c_n|^2$ are plotted together with their smoothed distribution $S_T(E)$ for $T = 0.04$. Some eigenstates lying under the bands have indeed somewhat larger probabilities, and considering these as a scar measure, one would expect that these eigenstates possess scars. In figures 10 to 13 the intensities of the four eigenstates with the largest probabilities $|c_n|^2$ are shown. Figure 10 shows the wavefunction with the highest value of $|c_n|^2$ having energy $E = 1586.400$ (see figure 8) which displays indeed some enhanced intensities along the periodic orbit. However, these intensity structures have to be compared with the random wave model to settle the issue whether these structures differ significantly from randomly generated ones. The figures 11 to 13 show the next to "best" scar candidates. These eigenstates show already less strikingly enhanced intensities near the periodic orbit. This is clearly a consequence of the fact that the burden to generate high intensities near the considered periodic orbit is shared by too many eigenstates.

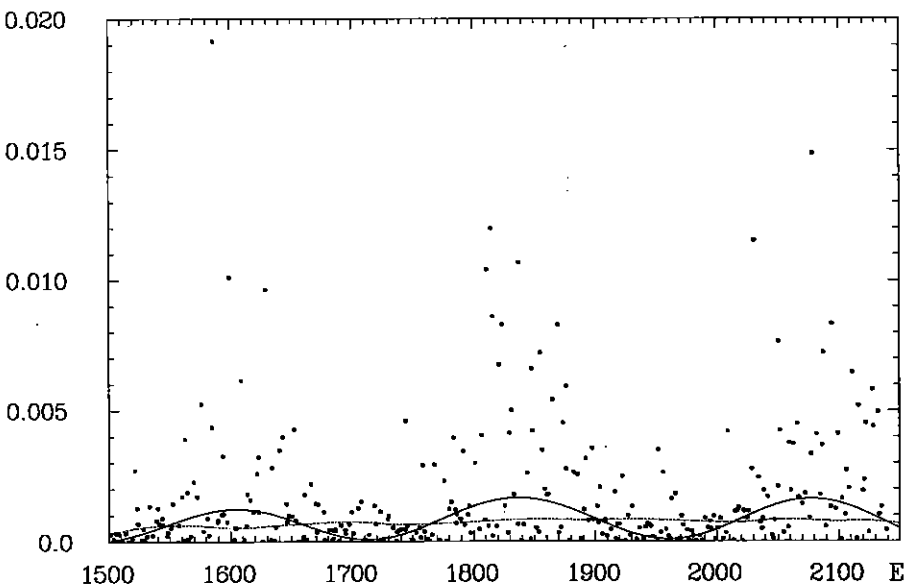

Figure 8: The probabilities $|c_n|^2$ are plotted in the energy range $1500 \leq E \leq 2140$, comprising 317 eigenstates with positive parity. In addition the smeared weighted spectral density $S_T(E)$, eq.(11), obtained from these probabilities is shown for $T = 0.04$ as a full curve. The dotted curve shows $S_T(E)$ calculated from the coefficients of the random wavefunctions which reflects no regular band structure.

The values of the highest probabilities are not larger than the values produced by the ran-

dom wavefunctions which know, however, nothing about any periodic orbit. In [8] the quantum eigenstates were expanded in terms of Legendre functions, and the expansion coefficients with respect to this basis were shown to be Gaussian distributed. This fact offers a simple method to generate random wavefunctions. The expansion coefficients with respect to the basis of Legendre functions are generated by a random–number generator according to a Gaussian distribution. This generates then a wavefunction which obeys the free Schrödinger equation, since the basis functions obey it. However, these wavefunction do not obey the periodic–boundary conditions, since this is only possible for the true eigenstates. Nevertheless, statistical properties like the amplitude distribution $P(\Psi)$ are the same for the true eigenstates and the random wavefunctions, since these properties are closely connected with the distribution of the expansion coefficients [8]. The important point for a comparison with respect to scars is that a random wavefunction cannot know anything about periodic orbits of the given hyperbolic octagon since it knows nothing about the periodic–boundary conditions by which the octagon is defined. In the energy range from $E = 1500$ to $E = 2140$ we have generated 520 random wavefunctions and computed their overlap integral with the wavepacket at $t = 0$, i. e. the coefficients c_n one would obtain if the wavepacket would be expanded into the random wavefunctions and if the random wavefunctions would constitute a complete basis. In figure 9 we show a comparison of the cumulative distribution of the probabilities $|c_n|^2$ of the true eigenstates and of the random wavefunctions. Both distributions agree well, and the Kolmogorov–Smirnov test yields a significance level of 41% that both distributions are identical. To avoid misunderstanding we note that the distributions of the c_n's are the same but not the locations at which they occur, because the c_n's of the true eigenstates possess larger magnitudes under the bands but not the c_n's of the random wavefunctions, which possess no band structure as figure 8 (dotted curve) reveals. It looks as if the theory based on the wavepacket dynamics leads only to a sorting of the c_n's with respect to the bands, but does not alter their magnitude. There occur again some large coefficients c_n due to random wavefunctions which would be scar candidates. The four random wavefunctions with the highest probabilities $|c_n|^2$ are shown in figures 14 to 17. A closer inspection shows clearly that the intensity structures of the random wavefunctions look similar to the four best scar candidates of the true eigenstates displayed in figures 10 to 13. The "best" random wavefunction (figure 14) shows an even more pronounced scar than any of the true wavefunctions. We thus conclude that there are no scars in highly excited eigenstates since the intensity structures seen in the true eigenstates do not differ in a statistically significant way from those seen in the random wavefunctions.

VII Summary and Discussion

In this paper we have studied highly excited quantum eigenstates with respect to the scar phenomenon which should endow the eigenstates with an enhanced structure according to Heller's scar model. The strongly chaotic system considered by us consists classically of a point particle sliding freely on a hyperbolic octagon. For the chosen hyperbolic octagon all eigenstates with energies $E_n \in [1500, 2140]$ and positive parity have been computed. The obtained 317 eigenstates have been the basis of our scar analysis.

The central point of Heller's scar model is provided by the dynamical properties of a localized wavepacket being launched along a short periodic orbit. The autocorrelation $C(t)$ reflects the periodicity of the chosen trajectory for times of the order of the period. This in turn enforces a band structure of the smeared weighted spectral density $S_T(E)$ which carries over to the individual weights $|c_n|$, i. e. the overlap of the localized wavepacket with the eigenstates. If

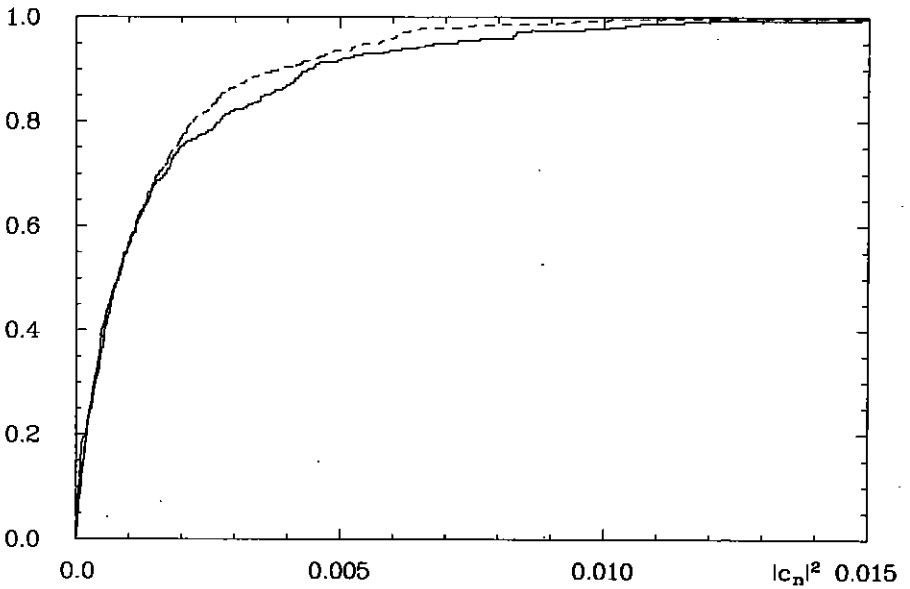

Figure 9: The cumulative distribution of the probabilities $|c_n|^2$ of the quantum eigenstates (full curve) is shown in comparison with the distribution obtained from the random wavefunctions (dashed curve).

only a very limited number of very large $|c_n|$'s occurs, the corresponding eigenstates must generate the localized wavepacket and have also to be localized. If, however, no small subset of eigenstates is selected by the $|c_n|$'s then many eigenstates share the burden to generate the localization along the periodic orbit, and no scar can be expected. This is exactly the case for hyperbolic octagons where already the number $N_b = \lambda \overline{d}(E)$ of quantum states lying under a single band is very large, e. g. for $E = 2000$, as discussed in the preceding sections, one obtains with $\lambda = 2p$ and $\overline{d}(E) = \frac{1}{2}$ the value $N_b \simeq 44$. Furthermore, with increasing energy the number of states under a single band increases, $N_b \simeq \sqrt{E}$, which suggests that in the semiclassical limit no scarred eigenstates can be expected. Since there are several bands, more than one hundred eigenstates contribute, and no trace of a scar should be left. Only for chaotic systems with very small N_b's one can expect scarred eigenstates.

To investigate the possibility that some quantum eigenstates could have nevertheless an intensity structure near short periodic orbits which differs significantly from the statistically expected one, we have created a random wavefunction model. A comparison of the random wavefunctions with the quantum eigenstates shows no statistically significant difference. Indeed, a comparison of the distributions of the $|c_n|$'s shows that both are identical with a high significance level of 41% obtained from the Kolmogorov–Smirnov test. Since the random wavefunction model knows nothing about periodic orbits, the existence of eigenstates which are scarred by periodic orbits is very improbable in the case of hyperbolic octagons.

Acknowledgement

We would like to thank the Deutsche Forschungsgemeinschaft for financial support and the HLRZ at Jülich for the access to the CRAY Y-MP 832 computer.

References

[1] E. P. Wigner, Phys. Rev. **40**(1932) 749.

[2] G. A. Baker, Phys. Rev. **109**(1958) 2198.

[3] A. I. Shnirelman, Usp. Mat. Nauk. **29**(1974) 181.

[4] A. Voros, Ann. Inst. H. Poincaré **24 A**(1976) 31.

[5] M. V. Berry, J. Phys. **A 10**(1977) 2083; Phil. Trans. Roy. Soc. **A 287**(1977) 237; Semiclassical Mechanics of Regular and Irregular Motion, in: Les Houches Summer School, Sect. XXXVI, G. Iooss,R. H. G. Helleman and R. Stora, eds. (North–Holland, Amsterdam, 1983), p.171.

[6] S. W. Mc Donald and A. N. Kaufmann, Phys. Rev. A **37**(1988) 3067.

[7] R. Aurich and F. Steiner, Physica **D 48**(1991) 445.

[8] R. Aurich and F. Steiner, Physica **D 64**(1993) 185.

[9] D. A. Hejhal and B. Rackner, University of Minnesota Supercomputer Institue Research Report UMSI 92/162.

[10] E.J.Heller, Phys. Rev. Lett. **53**(1984) 1515;
Springer Lecture Notes in Physics **263**(1986) 162.

[11] E. J. Heller, Wavepacket dynamics and quantum chaology, In *Proceedings of the 1989 Les Houches school on Chaos and Quantum Physics*, (eds. M. J. Giannoni, A. Voros and J. Zinn–Justin) Elsevier, Amsterdam 1991.

[12] D. Wintgen and A. Hönig, Phys. Rev. Lett. **63**(1989) 1467.

[13] D. Biswas, S. Pal and A. K. Chaundhuri, Phys. Rev. **A 45**(1992) 6185.

[14] P. Sarnak, Schur Lectures "Arithmetic Quantum Chaos", Tel–Aviv 1992.

[15] M. C. Gutzwiller, *"Chaos in Classical and Quantum Mechanics"*, Springer, New York (1990).

[16] N. L. Balazs and A. Voros, Phys. Rep. **143**(1986) 109.

[17] R. Aurich and F. Steiner, Physica **D 39**(1989) 169.

[18] R. Aurich and F. Steiner, Physica **D 43**(1990) 155.

[19] E. B. Bogomolny, Physica **D 31**(1988) 169.

[20] M. V. Berry, Some quantum–to–classical asymptotics, In *Proceedings of the 1989 Les Houches school on Chaos and Quantum Physics*, (eds. M. J. Giannoni, A. Voros and J. Zinn–Justin) Elsevier, Amsterdam 1991.

[21] M. Abramowitz and I. E. Stegun, *"Handbook of Mathematical Functions"*, Dover, New York (1965).

[22] C. Grosche and F. Steiner, Annals of Phys. **182**(1988) 120.

[23] R. Aurich and J. Bolte, Mod. Phys. Lett. **B 6**(1992) 1691.

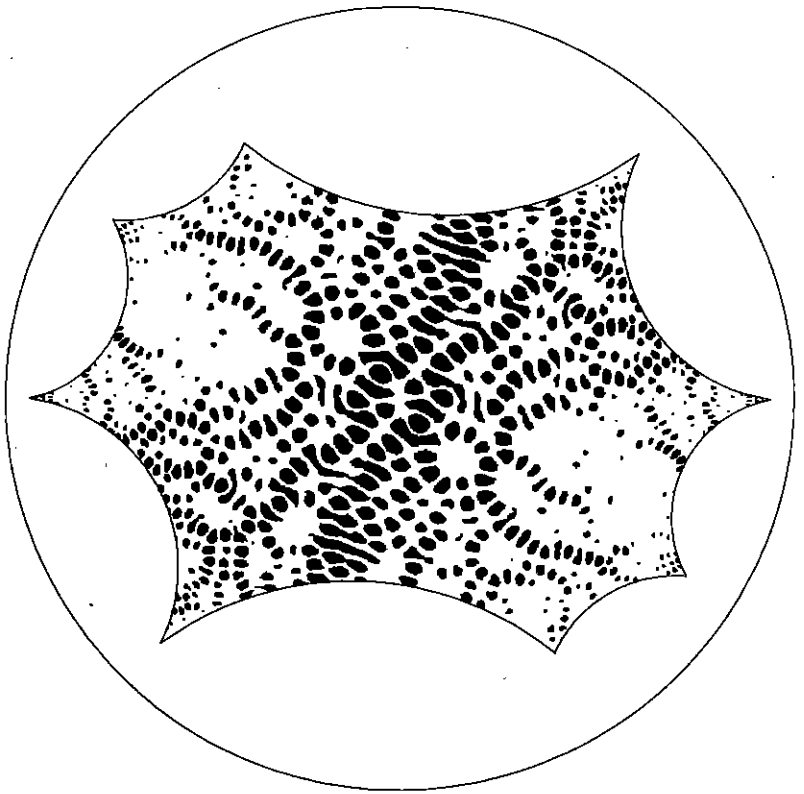

Figure 10: The intensity $|\Psi_n(z)|^2$ of the eigenstate at energy $E = 1586.400$ is shown in the Poincaré disc, whose boundary $|z| = 1$ is presented by the circle. The intensity is plotted in black, if it is above the threshold value $-\ln(c/\sqrt{2})/2\pi$ with $c = 0.6$.

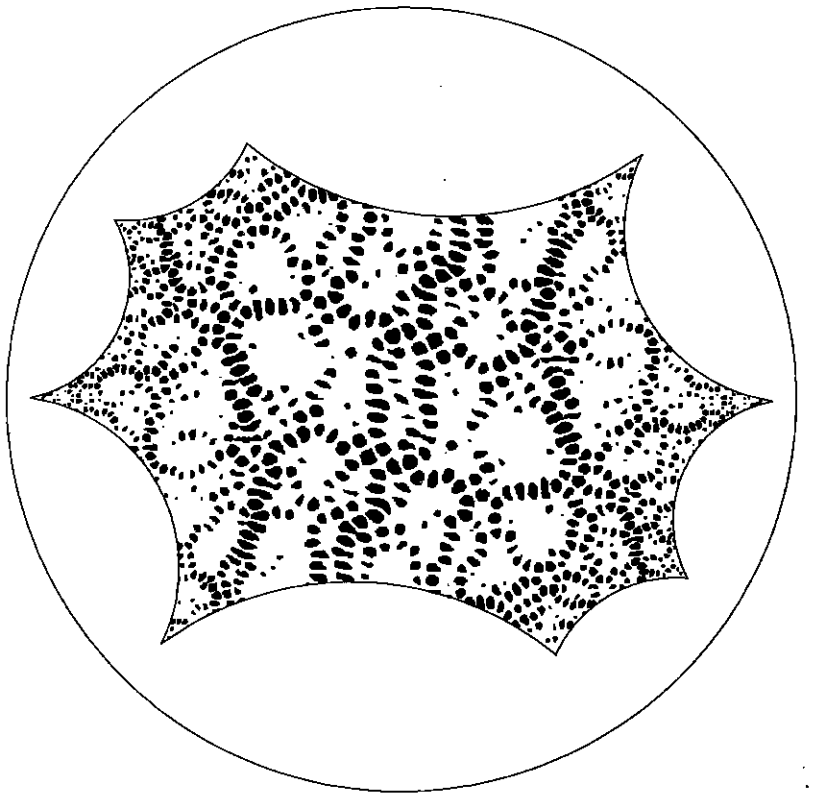

Figure 11: The same as in figure 10 for the eigenstate at energy $E = 2078.757$.

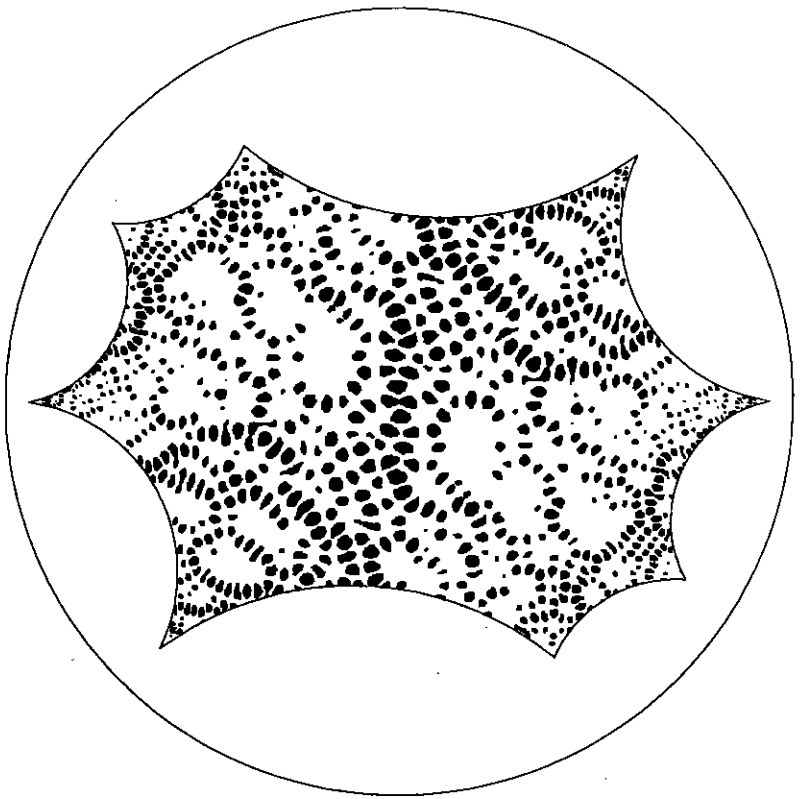

Figure 12: The same as in figure 10 for the eigenstate at energy $E = 1814.641$.

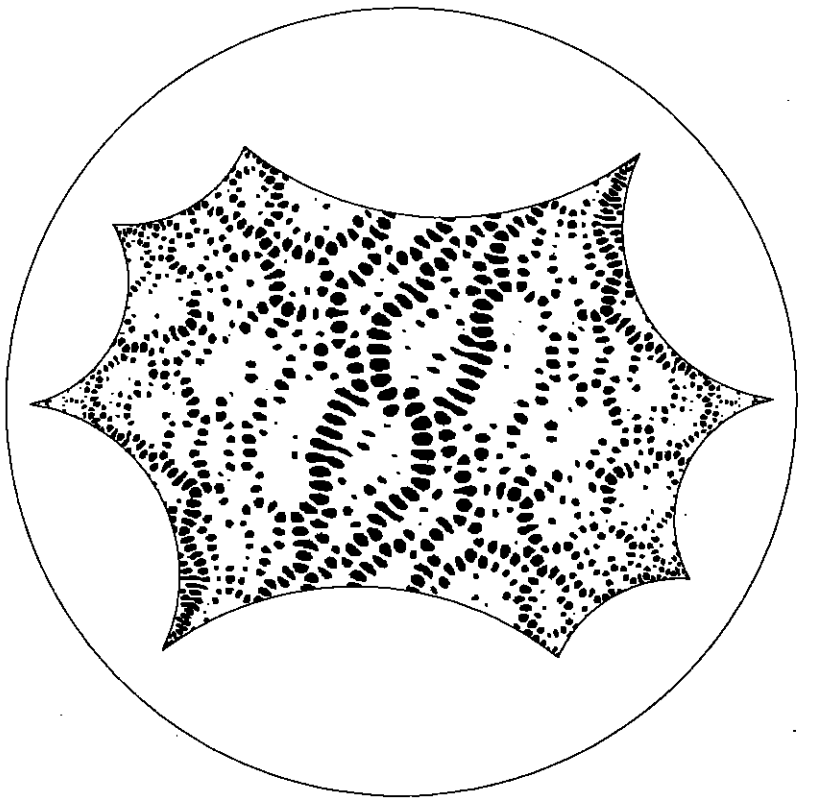

Figure 13: The same as in figure 10 for the eigenstate at energy $E = 2030.883$.

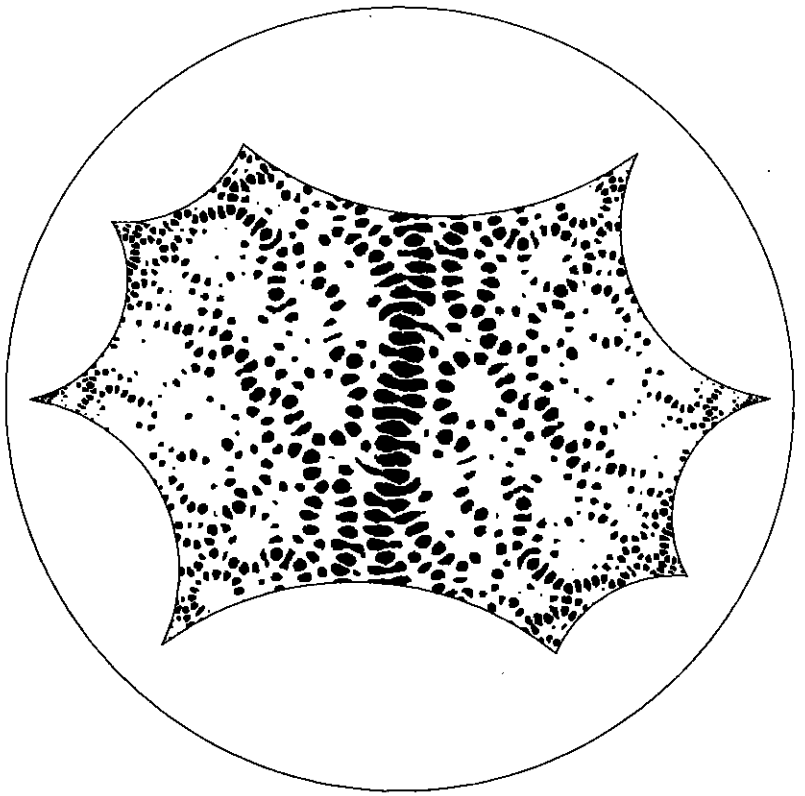

Figure 14: The random wavefunction with the largest overlap with the Gaussian wavepacket at energy $E = 1700$.

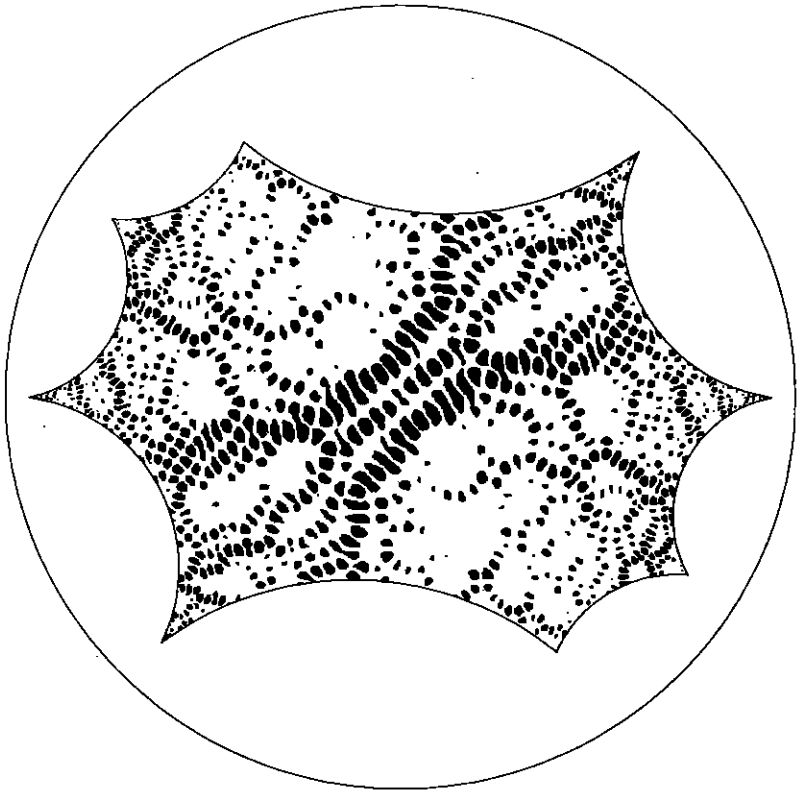

Figure 15: The random wavefunction with the second largest overlap with the Gaussian wavepacket at energy $E = 2137.5$.

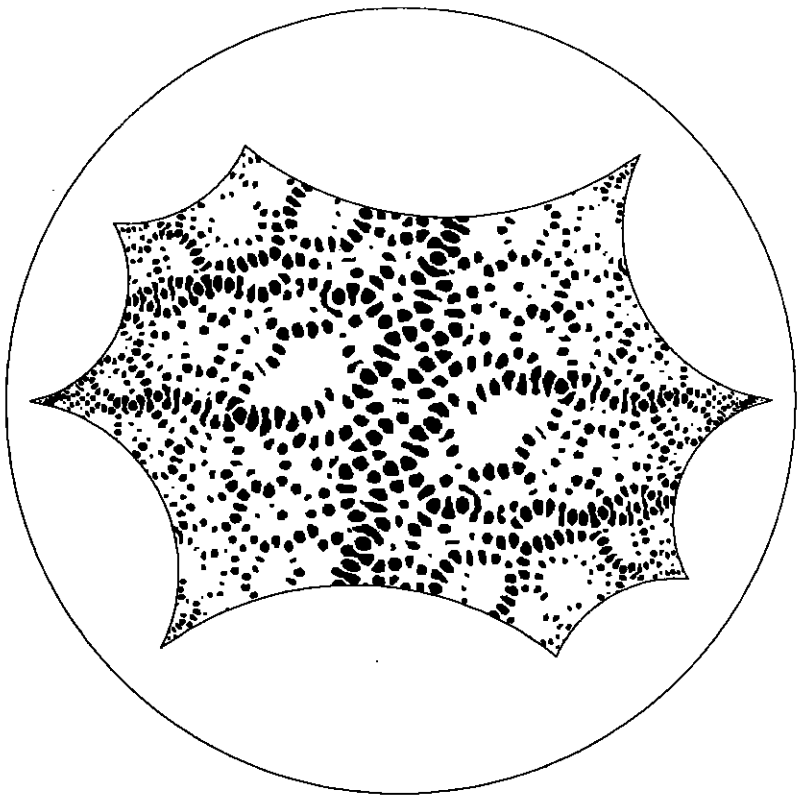

Figure 16: The random wavefunction with the third largest overlap with the Gaussian wavepacket at energy $E = 1925$.

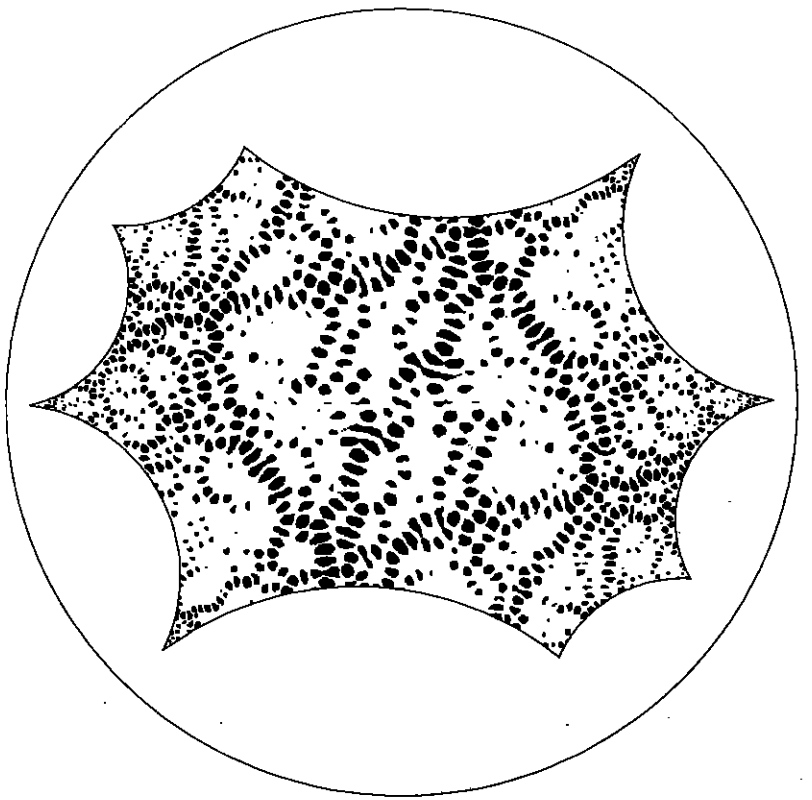

Figure 17: The random wavefunction with the fourth largest overlap with the Gaussian wavepacket at energy $E = 2137.5$.